



OPEN

Adsorption behaviors and mechanisms of Cu^{2+} , Zn^{2+} and Pb^{2+} by magnetically modified lignite

Junzhen Di, Zhen Ruan[✉], Siyi Zhang, Yanrong Dong, Saiou Fu, Hanzhe Li & Guoliang Jiang

The study aims to solve the problems of limited capacity and difficult recovery of lignite to adsorb Cu^{2+} , Zn^{2+} and Pb^{2+} in acid mine wastewater (AMD). Magnetically modified lignite (MML) was prepared by the chemical co-precipitation method. Static beaker experiments and dynamic continuous column experiments were set up to explore the adsorption properties of Cu^{2+} , Zn^{2+} and Pb^{2+} by lignite and MML. Lignite and MML before and after the adsorption of heavy metal ions were characterized by scanning electron microscopy (SEM), X-ray diffraction (XRD) and Fourier transform infrared spectrometer (FTIR). Meanwhile, the adsorption mechanisms of Cu^{2+} , Zn^{2+} and Pb^{2+} by lignite and MML were revealed by combining the adsorption isotherm model and the adsorption kinetics model. The results showed that the pH, adsorbent dosage, temperature, initial concentration of heavy metal ions, and contact time had an influence on the adsorption of Cu^{2+} , Zn^{2+} and Pb^{2+} by lignite and MML, and the adsorption processes were more in line with the Langmuir model. The adsorption kinetics experiments showed that the adsorption processes were jointly controlled by multiple adsorption stages. The adsorption of heavy metal ions by lignite obeyed the Quasi first-order kinetic model, while the adsorption of MML was chemisorption that obeyed the Quasi second-order kinetic model. The negative ΔG and positive ΔH of Cu^{2+} and Zn^{2+} indicated the spontaneous and endothermic nature reaction, while the negative ΔH of Pb^{2+} indicated the exothermic nature reaction. The dynamic continuous column experiments showed that the average removal rates of Cu^{2+} , Zn^{2+} and Pb^{2+} by lignite were 78.00, 76.97 and 78.65%, respectively, and those of heavy metal ions by MML were 82.83, 81.57 and 83.50%, respectively. Compared with lignite, the adsorption effect of MML was better. As shown by SEM, XRD and FTIR tests, Fe_3O_4 was successfully loaded on the surface of lignite during the magnetic modification, which made the surface morphology of lignite coarser. Lignite and MML removed Cu^{2+} , Zn^{2+} and Pb^{2+} from AMD in different forms. In addition, the adsorption process of MML is related to the O–H stretching vibration of carboxylic acid ions and the Fe–O stretching vibration of Fe_3O_4 particles.

In the process of coal mining, the original reduction environment can be changed into oxidation environment. Under the action of bacteria and oxygen, the existing sulfide can produce a large number of acid substances, which are dissolved in water and to form acid mine wastewater (AMD)¹. AMD has multiple hazards to the natural environment, embodied in low pH value, high sulfate concentration and heavy metal ion content². Among them, heavy metal ions such as Cu^{2+} , Zn^{2+} , and Pb^{2+} cannot be biodegraded or metabolized. After a series of food chain conduction, these heavy metal ions can be easily ingested into human body, and causing many health threat^{3,4}. Therefore, it is necessary to find some reliable methods to remove heavy metal ions such as Cu^{2+} , Zn^{2+} , and Pb^{2+} from AMD.

The treatment methods of heavy metal pollution in AMD mainly include chemical precipitation, microbial, wetland and adsorption method^{5–8}. Among them, adsorption method has the advantages of simple operation and treatment efficiency, which is widely used in the field of water treatment^{9,10}. Zendelska et al.¹¹ treated Zn^{2+} in AMD with zeolite-bearing tuff (stilbite) and analyzed the influence of each factor on the treatment effect through single factor experiment. Lin et al.¹² showed that spent shiitake substrate could be used to adsorb copper ions in AMD. Yang et al.¹³ used modified pyrite to conduct batch and column experiments to study its adsorption capacity for copper in simulated and actual AMD. Lin et al.¹⁴ used coffee grounds as adsorbent to adsorb Pb^{2+}

School of Civil Engineering, Liaoning Technical University, Fuxin 123000, China. ✉email: zhenruanlntu@126.com

and Zn^{2+} in AMD. The results showed that the maximum adsorption capacity of coffee grounds for Pb^{2+} and Zn^{2+} was 5.49 and 12.38 mg/g, respectively. At present, there are a variety of adsorption materials used to treat heavy metal ions in AMD, but there are problems of high treatment dosage and cost. Therefore, looking for an economical and reliable adsorption material has become a hot topic in the current field.

Lignite is rich in resources and low in price, mainly used in power plant fuel. However, lignite combustion seriously pollutes the air environment, which limits its use to a certain extent. Mohan et al.¹⁵ confirmed that lignite can be used as an adsorbent, which is rich in humic acid and has oxygen-producing functional groups such as carboxyl, hydroxyl and methoxyl, and has certain adsorption effect on heavy metal ions^{16,17}. Jellali et al.¹⁸ showed that lignite could remove cadmium and copper from aqueous solution under static experimental conditions, and the removal of cadmium accounted for 78% of the total adsorption capacity within one minute. Munir et al.¹⁹ applied bamboo biochar and lignite together, and explored the effect of bamboo biochar/lignite on the removal of copper ions in pore water by comparing the uptake of copper ions by rapeseed and wheat before and after application. However, the primary lignite has complex composition, single void structure and limited adsorption capacity for heavy metal ions. In order to improve the adsorption performance of lignite, many scholars have modified lignite. Sakthivel et al.²⁰ used facile depolymerization and Friedel Craft's alkylation to improve the wettability of lignite, and the removal rate of Cr(VI) of chemically modified lignite was still as high as 90–95% after 4–5 desorption tests. Regassa et al.²¹ treated lignite with acid, and the removal rate of Cr(VI) from acid-modified lignite could reach 98% under certain conditions. He et al.²² prepared copper-containing adsorbents by ultrasonic impregnation protocol and lignite as precursor, and calculated by Langmuir isothermal model that the maximum adsorption capacity of direct yellow brown D3G in wastewater at 25 °C was 369 mg/g. These studies further confirm the potential of lignite in the field of adsorption.

Although lignite can be modified to improve its adsorption performance, it is difficult to precipitate and separate lignite in wastewater treatment due to its suspension. Cheng et al.²³ used chitosan as bridging reagent to prepare magnetic Fe_3O_4 particle modified sawdust, which can be quickly separated from the solution and has a maximum adsorption capacity of 12.59 mg/g for strontium ions in the solution. The magnetic natural composite Fe_3O_4 -chitosan@bentonite synthesized by Feng et al.²⁴ can be easily recovered by external magnetic field after AMD treatment. Moreover, the adsorption capacity of Cr(VI) decreased only 3% after five consecutive adsorption–desorption processes. Chen et al.²⁵ modified attapulgite with hydrochloric acid and mixed it with Fe_3O_4 to prepare adsorption material for Cr(VI) treatment in water. The study shows that the removal rate of Cr(VI) is as high as 95% within 5 min, and it can be easily removed from aqueous solution by external magnetic field after treatment. The above researches show that loading magnetic source of Fe_3O_4 onto the surface of solid particles can not only solve the problem of difficult separation of powder adsorbent with large specific surface area which from the target solution, but also improve the adsorption performance of the adsorbent. Based on the above considerations, functionalization of lignite with Fe_3O_4 can be considered for the removal of heavy metal ions in AMD.

In this paper, magnetically modified lignite (MML) was prepared by chemical co-precipitation method and used to remove Cu^{2+} , Zn^{2+} and Pb^{2+} from AMD. The removal effects of Cu^{2+} , Zn^{2+} and Pb^{2+} by Lignite and MML in AMD were compared by static beaker experiments and dynamic continuous column experiments, and the lignite and MML materials before and after the adsorption of heavy metal ions were characterized by SEM, XRD and FTIR. At the same time, the adsorption mechanisms of Cu^{2+} , Zn^{2+} and Pb^{2+} by lignite and MML were revealed by combining the adsorption isotherm model and the adsorption kinetics model. Through this study, it can not only solve the problem that lignite is difficult to separate from solution, but also improve the ability of lignite to adsorb heavy metal ions. The treatment of AMD has significant environmental, social and economic benefits.

Results and discussion

Effect of pH, adsorbent dose and temperature. *Effect of pH.* According to the actual pH of AMD, the effects of different pH (2–4) on the adsorption process of Cu^{2+} , Zn^{2+} and Pb^{2+} by lignite and MML were studied as shown in Fig. 1a,b. With the increase of pH value, the adsorption of Cu^{2+} , Zn^{2+} and Pb^{2+} by lignite and MML gradually increases. When pH=4, the removal rates of heavy metal ions reaches the maximum. Among them, the removal rates of Cu^{2+} , Zn^{2+} and Pb^{2+} by lignite are 83.02, 78.79 and 80.34%, respectively, and those of heavy metal ions by MML are 91.61, 89.60 and 98.00%, respectively. It can be seen that MML has higher adsorption capacity than lignite. In addition, the results show that pH has a great influence on the adsorption process. Because large amount of H^+ in a strong acidic solution would compete with heavy metal cations for adsorption sites, leading to the low removal rates under lower pH value. Therefore, the optimum pH value is 4.

Effect of adsorbent dose. The effects of different adsorbent dosage on the adsorption process of Cu^{2+} , Zn^{2+} and Pb^{2+} were studied as shown in Fig. 1c,d. It can be seen that with the increase of adsorbent amount, the removal rates also increases. For MML, when the adsorbent amount is 4 g/L, the removal rates of heavy metal ions exceeds 89%. When the amount of MML is increased to 6 g/L, the reaction tends to be balanced, and the removal rates is not significantly improved. Therefore, considering the adsorption effect and economic cost, the optimum adsorbent amount is 1 g/L.

Effect of temperature. Temperature is an important parameter in the adsorption process. The effects of temperature on the adsorption process of heavy metal ions at different temperatures (298.15, 308.15 and 318.15 K) were shown in Fig. 1e,f. The removal rates of Cu^{2+} and Zn^{2+} by lignite and MML increases with the increase of temperature, indicating that the adsorption process is endothermic. However, the removal rate of Pb^{2+} decreases with the increase of temperature, which indicates that the adsorption process of Pb^{2+} by lignite and MML is exothermic. Although the removal rates of Cu^{2+} and Zn^{2+} by lignite and MML reaches the maximum at 318.15

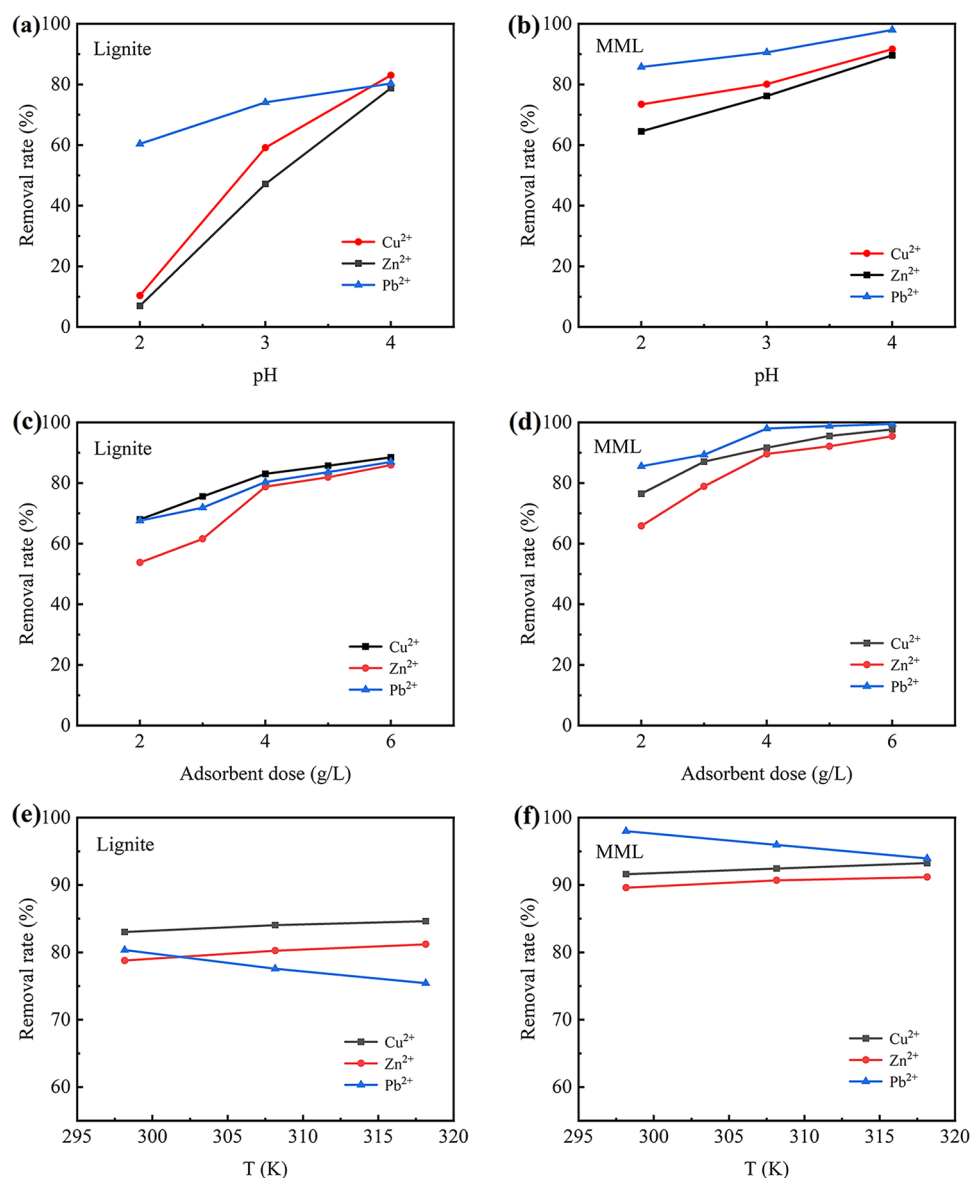


Figure 1. Relationship between the pH value and adsorption effect: (a) lignite; (b) MML. Relationship between adsorbent dose and adsorption effect: (c) lignite; (d) MML. Relationship between temperature and adsorption effect: (e) lignite; (f) MML.

K (i.e. 45 °C), most reaction systems are carried out at ambient temperature, so the optimum temperature is 298.15 K (i.e. 25 °C).

Initial concentration and adsorption isotherm. *Effect of initial concentration.* The adsorption capacity and removal rates of lignite and MML for different initial concentrations of heavy metal ions were shown in Fig. 2. The adsorption capacity of heavy metal ions by lignite and MML increases with the increase of initial concentration.

This is because the higher the initial concentration of heavy metal ions, the higher the chance of collisions with adsorption sites on the surface of the adsorbent. Moreover, the driving force of mass transfer is better, which is conducive to reduce the mass transfer resistance and increase the adsorption capacity²⁶. However, the removal rate of heavy metal ions by lignite and MML decreases with the increase of initial concentration. Especially when the initial concentration of Cu²⁺, Zn²⁺ and Pb²⁺ are 30, 30, and 50 mg/L respectively, the slope of the removal rate curve increases significantly. This is because for the fixed amount of adsorbent, the number of adsorption sites on the surface is limited, and the adsorption effect will achieve the best adsorption at a certain concentration of heavy metal ions.

Comparing the adsorption effects of lignite and MML on heavy metal ions, it can be seen that the adsorption capacity and removal rates of Cu²⁺, Zn²⁺ and Pb²⁺ by MML are higher than that of lignite at the same concentrated

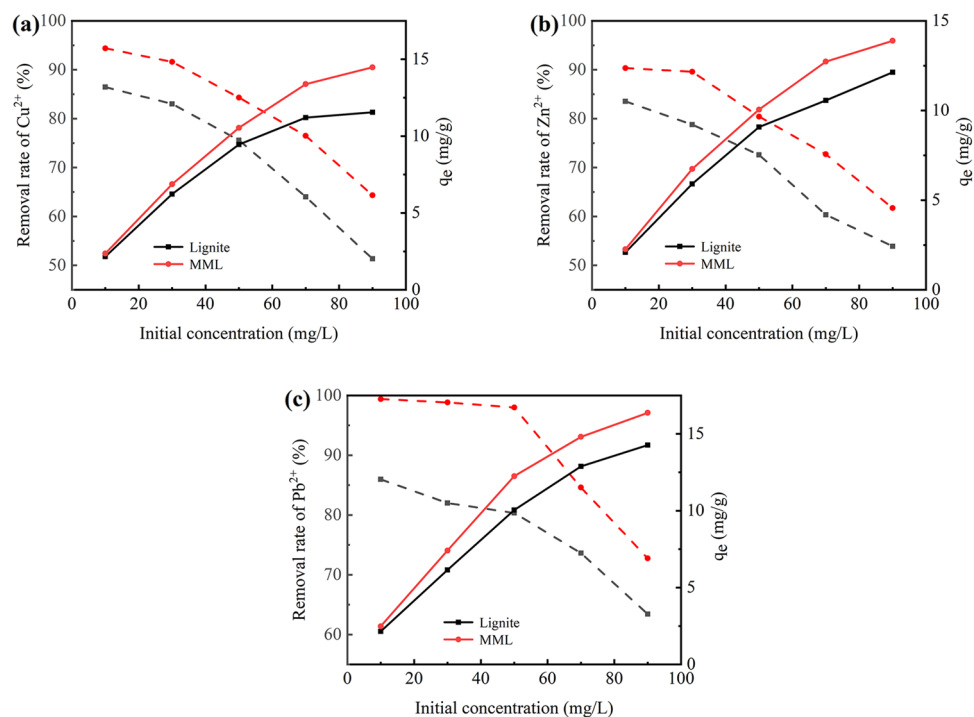


Figure 2. Relationship between initial concentration of heavy metal ions and adsorption effect: (a) Cu²⁺ removal effect; (b) Zn²⁺ removal effect; (c) Pb²⁺ removal effect.

heavy metal ion degree. In the initial concentration range of 10–90 mg/L, the removal rates of Cu²⁺ and Zn²⁺ by lignite and MML shows similar trends, and the difference in removal rates tend to increase. In contrast, the removal rates of Pb²⁺ by MML in the range of 10–50 mg/L is almost constant with increasing initial concentration, indicating that Pb²⁺ in AMD is well removed by MML in this range. In addition, In the initial concentration range of 10–90 mg/L, the difference of adsorption of Cu²⁺, Zn²⁺ and Pb²⁺ between MML and lignite increases with the increase of initial concentration. This phenomenon indicates that MML has greater adsorption potential than lignite when the concentration of heavy metal ions in AMD solution is higher.

Adsorption isotherm. The adsorption isotherm describes the relationship between the adsorbent and the amount of analytical substances in the solution²⁷. To clarify the mechanism of Cu²⁺, Zn²⁺ and Pb²⁺ adsorption by lignite and MML, the Langmuir model and Freundlich model were used to fit the experimental data.

The Langmuir model assumes that monolayer adsorption occurs on the uniform adsorbent surface, with no interaction between adsorbates. The Langmuir model is expressed in the following form²⁸:

$$\frac{C_e}{q_e} = \frac{C_e}{q_m} + \frac{1}{(K_L q_m)} \quad (1)$$

where q_m and q_e are the maximum adsorption capacity and the adsorption capacity at equilibrium (mg/g), respectively, C_e is the adsorbate concentration in solution at equilibrium (mg/L), and K_L is the Langmuir adsorption constant (L/mg). The values of q_m and K_L can be calculated by a linear relationship. In addition, the equilibrium constant R_L of the Langmuir model can be used to describe the adsorption effect of the adsorption process. The R_L equation is of the following form²⁹:

$$R_L = \frac{1}{1 + K_L C_0} \quad (2)$$

where C_0 is the initial concentration of metal ions. The value $R_L < 1$ indicates good adsorption performance.

Based on multilayer adsorption on non-homogeneous surfaces, the empirical Freundlich equation without assumptions is expressed in the following form³⁰:

$$\ln q_e = \ln K_F + \frac{1}{n} \ln C_e \quad (3)$$

where K_F (L/mg) and n (dimensionless) are constant indications of the adsorption capacity.

The adsorption isotherms and corresponding parameters of Cu²⁺, Zn²⁺ and Pb²⁺ adsorption by lignite and MML were shown in Fig. 3 and Table 1, respectively. The correlation coefficient ($R^2 > 0.99$) of the Langmuir model is higher, indicating that the processes of Cu²⁺, Zn²⁺ and Pb²⁺ adsorption by lignite and MML are more consistent

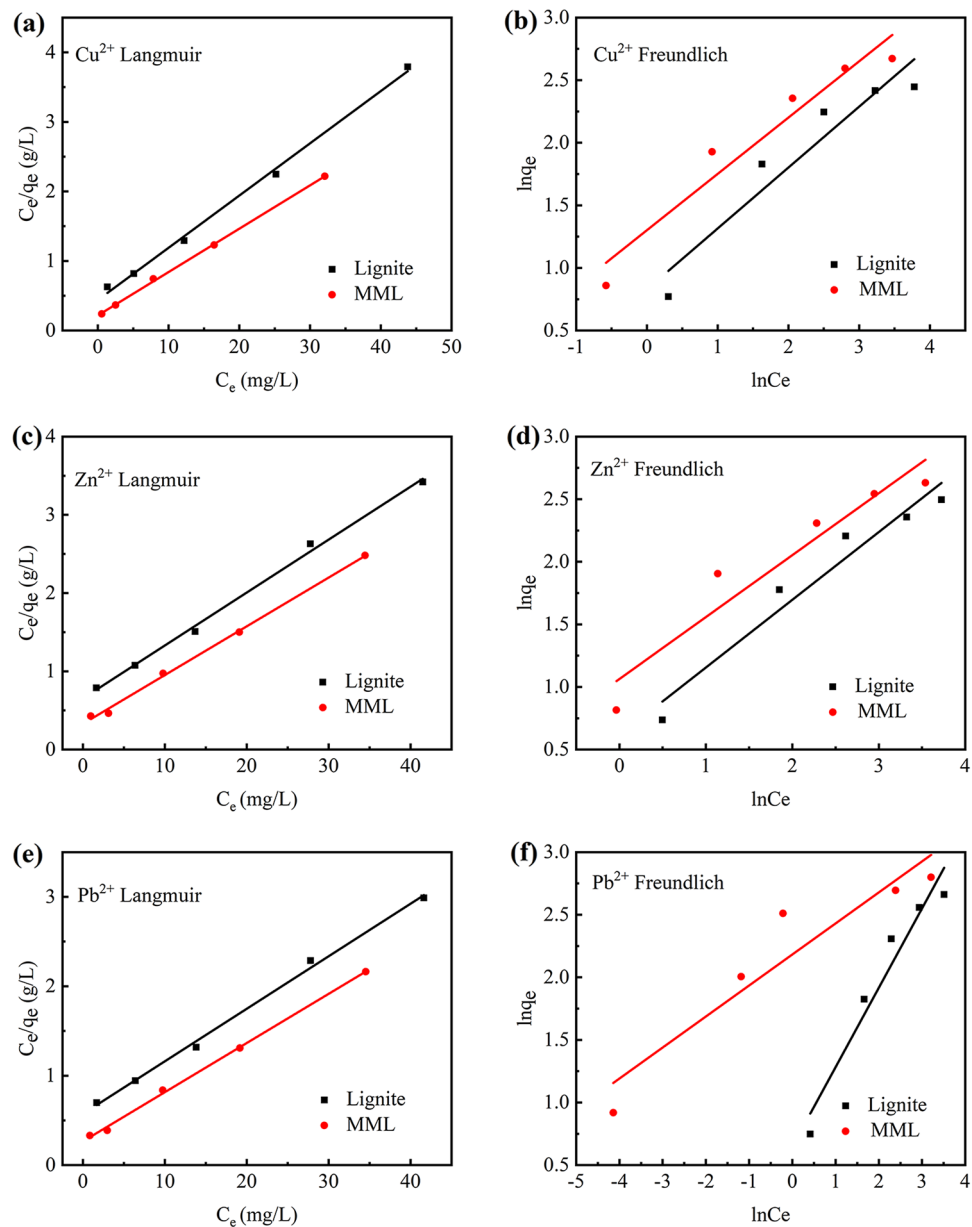


Figure 3. Linear plots of adsorption isotherms of heavy metal ion adsorption on different samples: lignite; MML. (a) Cu²⁺ Langmuir; (b) Cu²⁺ Freundlich; (c) Zn²⁺ Langmuir; (d) Zn²⁺ Freundlich; (e) Pb²⁺ Langmuir; (f) Pb²⁺ Freundlich.

Metal ion	Adsorption material	Langmuir				Freundlich			
		K _L (L/mg)	q _m (mg/g)	R ²	R _L	K _F (L/mg)	1/n	R ²	
Cu ²⁺	Lignite	0.16684	13.36180	0.99576	0.16652	2.26204	0.48950	0.88550	
	MML	0.25769	16.21270	0.99926	0.11458	3.47001	0.46680	0.91549	
Zn ²⁺	Lignite	0.10161	14.79290	0.99571	0.24702	1.82106	0.54410	0.93473	
	MML	0.20573	15.80530	0.99772	0.13943	3.03035	0.47940	0.92316	
Pb ²⁺	Lignite	0.09121	17.52740	0.98246	0.17984	1.90594	0.63730	0.92816	
	MML	0.25673	18.38700	0.99755	0.07227	8.85303	0.24820	0.85616	

Table 1. Adsorption isotherm constants for the adsorption of heavy metal ion onto different samples: lignite; MML.

with the Langmuir model (Table 1). On the basis of this result, it can be inferred that the processes of Cu^{2+} , Zn^{2+} and Pb^{2+} adsorption by lignite and MML belong to Langmuir monolayer adsorption, where there is no interaction between the heavy metal ions adsorbed on the surface³¹. This indicates that a monolayer adsorbent is formed on the surface of lignite and MML, and no further adsorption will be carried out after the surface is completely covered^{32,33}. In addition, the R_L value obtained according to Langmuir adsorption constant K_L is between 0 and 1, indicating that lignite and MML have good adsorption of heavy metal ions³⁴. In Freundlich model, the $1/n$ value less than 1 also confirms that the adsorption conditions is good, and a smaller $1/n$ value indicates that MML is more favorable for the adsorption of Cu^{2+} , Zn^{2+} and Pb^{2+} in the solution^{35,36}.

By comparing the parameters of lignite and MML adsorption isotherms, it can be seen that the Langmuir model of MML has a large correlation coefficient, which may be due to the uniform specific adsorption sites generated in the magnetization process³⁷. It has been reported that the larger the adsorption capacity of the adsorbent, the greater the K_F value³⁸. The K_F value of MML in this study is larger than that of original lignite, indicating that the adsorption capacity of MML is larger than that of lignite. The maximum adsorption capacity of MML for Cu^{2+} , Zn^{2+} and Pb^{2+} are 16.2127, 15.8053 and 18.3870 mg/g, respectively, while the maximum adsorption capacities of lignite are 13.3618, 14.7929 and 17.5274 mg/g, respectively. It is further confirmed that magnetic modification of lignite improves the adsorption capacity of Cu^{2+} , Zn^{2+} and Pb^{2+} .

Contact time and adsorption kinetics. To clarify the adsorption mechanism of lignite and MML, the adsorption kinetics of Cu^{2+} , Zn^{2+} and Pb^{2+} by lignite and MML were analyzed by Quasi first-order kinetic model, Quasi second-order kinetic model, Elovich model and Intra-particle diffusion model.

Quasi first-order model. Lagergren proposed an adsorption analysis method based on solid adsorption capacity²⁰, which is the Quasi first-order kinetic equation in the following form^{29,31}:

$$\ln(q_e - q_t) = \ln q_e - k_1 t \quad (4)$$

where q_e and q_t are the amounts of adsorbed metal ions at equilibrium and at time t (mg/g), respectively, and k_1 is the Quasi first-order rate constant (min^{-1}).

Quasi second-order model. The Quasi second-order kinetic model is based on the assumption that the adsorption rate is controlled by chemisorption²⁴. The Quasi second-order kinetic model is expressed in the following form³⁹:

$$\frac{t}{q_t} = \frac{1}{k_2 q_e^2} + \frac{t}{q_e} \quad (5)$$

where q_e and q_t are the amounts of adsorbed metal ions at equilibrium and at time t (mg/g), respectively, and k_2 is the Quasi second-order rate constant (min^{-1}).

The results of Quasi first-order model and Quasi-second-order kinetic fits for the adsorption of Cu^{2+} , Zn^{2+} and Pb^{2+} by lignite and MML were shown in Fig. 4 and Table 2.

From Fig. 4a,b, it can be seen that the tangent slope of the curve is larger at the beginning of the adsorption, indicating that the adsorption rate of MML and lignite to adsorb heavy metal ions is faster. Then the slope gradually decreases and the adsorption rate decreases. This is because there are enough effective adsorption sites on the surface of the adsorbent at the initial stage. As the reaction progresses, the adsorption sites are gradually occupied, resulting in the reduction of the adsorption efficiency. On the other hand, the experimental results (Fig. 4a) show that for the single-component mode, as reported by Jellali et al.¹⁸, the adsorption efficiency of the studied heavy metal ions by lignite is as follows: $\text{Pb}^{2+} > \text{Cu}^{2+} > \text{Zn}^{2+}$. However, for the single-component mode, the adsorption efficiency of the studied heavy metal ions by MML is as follows: $\text{Pb}^{2+} > \text{Zn}^{2+} > \text{Cu}^{2+}$ (Fig. 4b). This may be because the magnetic modification affected the physico-chemical properties of the lignite, such as the donor atoms abundance (oxygen, nitrogen, sulfur)⁴⁰.

As can be seen from Table 2, the Quasi first-order kinetic parameters R^2 for the adsorption of Cu^{2+} , Zn^{2+} and Pb^{2+} by lignite are higher ($R^2 > 0.96$), indicating that the adsorption process follows the Quasi first-order kinetic model and is dominated by physisorption⁴¹. The fitted equations of the Quasi first-order kinetics model of lignite for Cu^{2+} , Zn^{2+} and Pb^{2+} are: $y = 9.2602 \cdot (1 - e^{-0.00607x})$, $y = 10.2839 \cdot (1 - e^{-0.00468x})$, and $y = 11.8456 \cdot (1 - e^{-0.01265x})$, respectively. In contrast, the Quasi second-order kinetic parameter R^2 for the adsorption of heavy metal ions by MML is higher than that of the Quasi first-order kinetic, indicating that the Quasi second-order kinetic model fits well the experimental data for three heavy metal ions²⁵. Moreover, the Quasi second-order kinetic equilibrium adsorption capacity is closer to the experimental adsorption capacity. Therefore, under the used experimental conditions, the Quasi second-order kinetic model is more suitable for fitting the adsorption process of Cu^{2+} , Zn^{2+} and Pb^{2+} by MML. The Quasi second-order kinetic model shows that the adsorption process of the studied heavy metal ions by MML is mainly chemisorption, and the adsorption rate is affected by the coordination between the surface active site of adsorbent and the heavy metal ions⁴². The fitted equations for the Quasi second-order kinetics model of MML for Cu^{2+} , Zn^{2+} and Pb^{2+} are: $y = 0.09599x + 8.81861$, $y = 0.09333x + 10.01582$, and $y = 0.05103x + 5.02836$, respectively.

Elovich model. The Elovich model assumes that with the increase of the amount of heavy metal ions, the adsorption rate decreases exponentially, following a chemisorption mechanism. The model is expressed in the following form⁴³:

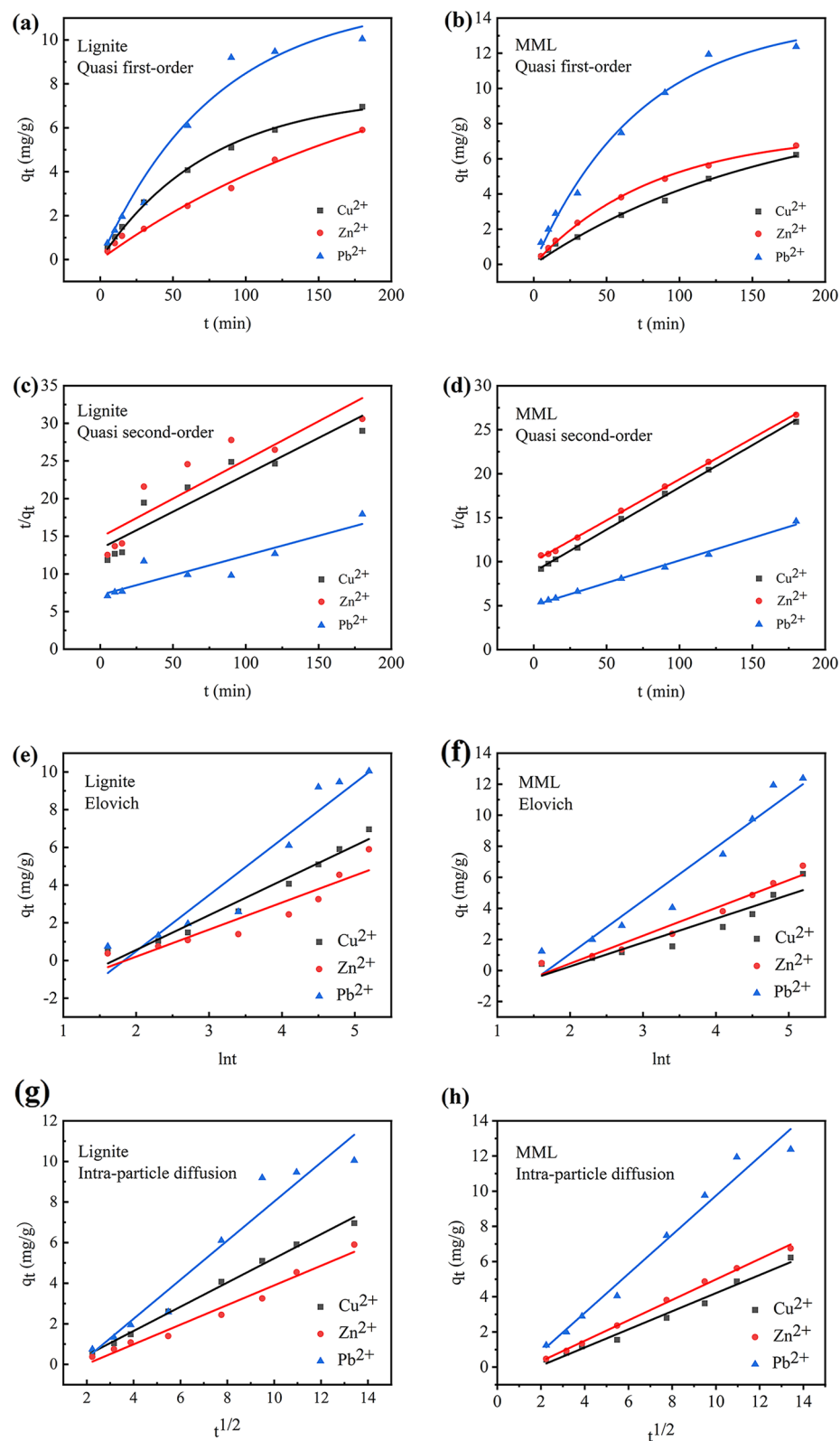


Figure 4. Adsorption kinetics for adsorption of Cu^{2+} , Zn^{2+} and Pb^{2+} onto different samples: lignite; MML. (a) Quasi first-order kinetic model of the adsorption of lignite; (b) quasi first-order kinetic model of the adsorption of MML; (c) quasi second-order kinetic model of the adsorption of lignite; (d) quasi second-order kinetic model of the adsorption of MML; (e) Elovich model of the adsorption of lignite; (f) Elovich model of the adsorption of MML; (g) intra-particle diffusion model of the adsorption of lignite; (h) intra-particle diffusion model of the adsorption of MML.

Metal ion	Adsorption material	Quas first-order model			Quasi second-order model			Elovich model			Intra-particle diffusion model		
		K ₁	q _e (mg/g)	R ²	K ₂	q _e (mg/g)	R ²	a	b	R ²	K ₃	C	R ²
Cu ²⁺	Lignite	0.00607	9.26020	0.98854	0.00072	10.19260	0.85585	0.33849	0.54289	0.96605	0.73173	-1.65400	0.87331
	MML	0.01311	7.53811	0.99724	0.00104	10.41780	0.99906	0.24709	0.65012	0.89240	0.87488	-1.72723	0.95551
Zn ²⁺	Lignite	0.00468	10.28394	0.98526	0.00070	9.74470	0.78164	0.22419	0.69708	0.87171	0.68009	-1.56120	0.84320
	MML	0.01191	7.52736	0.99828	0.00087	10.71470	0.99925	0.31145	0.55851	0.95981	0.85380	-1.78576	0.95279
Pb ²⁺	Lignite	0.01251	11.85742	0.96693	0.00038	19.03300	0.79657	0.47558	0.33625	0.91686	1.47048	-3.53485	0.98318
	MML	0.01327	14.01561	0.98903	0.00052	19.59630	0.99463	0.63466	0.29240	0.94079	1.63444	-3.37912	0.97145

Table 2. Kinetic parameters of heavy metal ion adsorption on different samples: lignite; MML.

$$q_t = \frac{1}{b} \ln(ab) + \frac{1}{b} \ln t \quad (6)$$

where a and b are Elovich constants.

The experimental data were fitted by the Elovich model, and the results were shown in Fig. 4 and Table 2. As can be seen, Elovich model is in good agreement with the experimental data of adsorption of Cu²⁺, Zn²⁺ and Pb²⁺ by lignite and MML, and R² is between 0.87 and 0.97 (Fig. 4e,f). It shows that there is chemisorption between adsorbents (lignite and MML) and three kinds of heavy metal ions.

Intra-particle diffusion model. The adsorption process usually involves two main mechanisms: film diffusion and particle diffusion. In order to determine the way of metal ions entering the adsorbent material from the solution, the Intra-particle diffusion model (Eq. 7) was used to determine the adsorption rate control steps and the results are shown in Fig. 4 and Table 2⁴⁴.

$$q_t = k_3 t^{1/2} + C \quad (7)$$

where q_t is the amount of metal ions adsorbed at any moment t (mg/g), k_3 is the diffusion rate constant within the particle (min⁻¹), and C is the constant involving thickness and boundary layer. The larger the value of C , the greater the contribution of the boundary layer.

Figure 4g,h show the linear relationship between q_t and $t^{1/2}$. Among them, the parameters of the Intra-particle diffusion model for Cu²⁺, Zn²⁺ and Pb²⁺ adsorption by lignite and MML were shown in Table 2. According to reports, if the plots are linear and pass through the origin, indicating that Intra-particle diffusion is the only rate control step; if the linear plot of the fitted results does not pass through the origin, indicating that the adsorption rate is also controlled by other adsorption stages⁴⁵. As can be seen in Fig. 4, the fitted results for the adsorption of Cu²⁺, Zn²⁺ and Pb²⁺ by lignite and MML are linear and do not pass the origin, indicating that the rates of Cu²⁺, Zn²⁺ and Pb²⁺ adsorption by lignite and MML are jointly controlled by multiple adsorption stages. In addition, linearity indicates spontaneous utilization of available adsorption sites on adsorbent surfaces³⁸.

Adsorption thermodynamics. Based on the adsorption experimental data affected by temperature, the thermodynamic parameters (Gibbs free energy changes, ΔG ; entropy, ΔS and enthalpy change, ΔH) determined in the following forms³⁷:

$$K = \frac{q_e}{c_e} \quad (8)$$

$$\Delta G = -RT \ln K \quad (9)$$

$$\ln K = \frac{\Delta S}{R} - \frac{\Delta H}{RT} \quad (10)$$

where R is the ideal gas constant (8.314 J/mol·K), T is the Kelvin temperature (K), and K is the thermodynamic equilibrium constant.

According to the experimental results, the thermodynamic parameters were determined, as shown in Fig. 5 and Table 3. The positive ΔH values of Cu²⁺ and Zn²⁺ indicates that the adsorption of Cu²⁺ and Zn²⁺ by lignite and MML is endothermic adsorption, while the negative ΔH values of Pb²⁺ indicates that the adsorption is exothermic adsorption. With the increase of temperature, the negative ΔG values of Cu²⁺ and Zn²⁺ become more negative, which indicates that the adsorption efficiency is higher at higher temperature and the adsorption is spontaneous. The negative ΔG values of Pb²⁺ tend to positive, indicating that the adsorption is spontaneous but its adsorption efficiency is lower at higher temperature. The results show that the temperature increase is beneficial to the adsorption of Cu²⁺ and Zn²⁺ by lignite and MML, but not conducive to the adsorption of Pb²⁺. In addition, the ΔG values of an adsorbent for the adsorption of some heavy metal ions at different temperatures are very close, which indicates that the adsorption process of Cu²⁺, Zn²⁺ and Pb²⁺ by lignite and MML is not obviously affected by temperature.

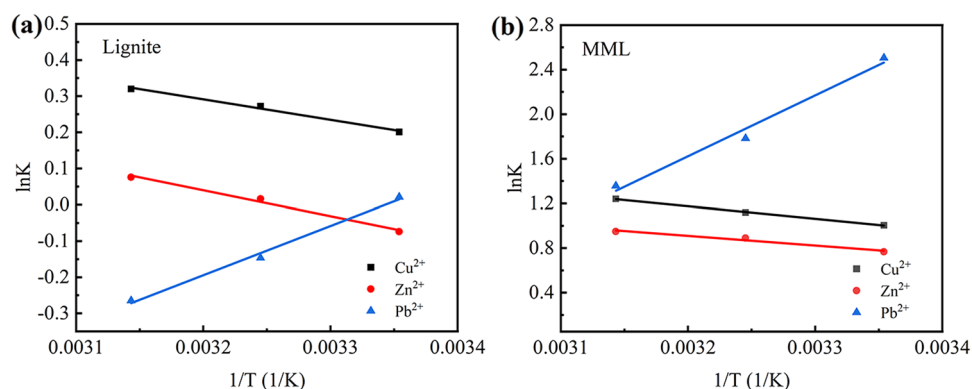


Figure 5. Relationship curve between $\ln K$ and $1/T$: (a) lignite; (b) MML.

Adsorption material	Metal ion	ΔH (kJ/mol)	ΔS (J/mol K)	ΔG (kJ/mol)		
				298.15 K	308.15 K	318.15 K
Lignite	Cu^{2+}	4.70583	17.48052	-0.49799	-0.69788	-0.846643
	Zn^{2+}	5.92687	19.29696	0.18368	-0.04125	-0.20076
	Pb^{2+}	-11.30457	-37.79145	-0.05280	0.37456	0.70069
MML	Cu^{2+}	9.26270	39.40279	-2.49072	-2.86760	-3.27939
	Zn^{2+}	7.19446	30.58529	-1.90175	-2.27912	-2.51020
	Pb^{2+}	-45.2219	-131.86095	-6.21069	-4.56951	-3.58834

Table 3. Thermodynamic parameters for adsorption of Cu^{2+} , Zn^{2+} and Pb^{2+} onto different samples: Lignite; MML.

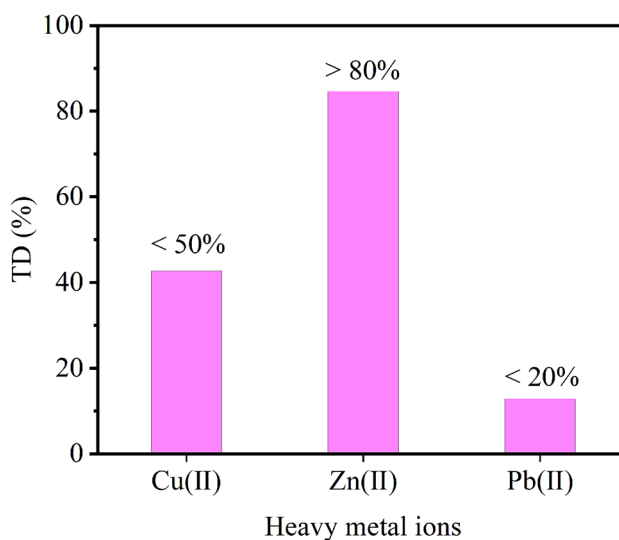


Figure 6. Desorption rate of heavy metal ions by MML.

Desorption. To clarify the properties of MML adsorption of Cu^{2+} , Zn^{2+} and Pb^{2+} , desorption experiments were used to analyze the adsorption process. The desorption agents commonly used for desorption of adsorbents are NaOH, HCl, HNO_3 , EDTA, CaCl_2 and organic solvents such as methanol and ethanol⁴⁶. In this study, 0.1 mol/L H_2SO_4 was used as desorption agent for desorption experiment. Figure 6 shows that the desorption rates of Cu^{2+} and Pb^{2+} are less than 50%, indicating that the retention of MML for both metals is very strong under acidic conditions. Therefore, the adsorption process of Cu^{2+} and Pb^{2+} by MML is chemisorption. This result is consistent with the adsorption kinetics. However, the desorption rate of Pb^{2+} is as high as 84.62%, which may be due to the removal of Zn^{2+} in the form of $\text{Zn}(\text{OH})_2$ in solution. When the pH value of the desorption

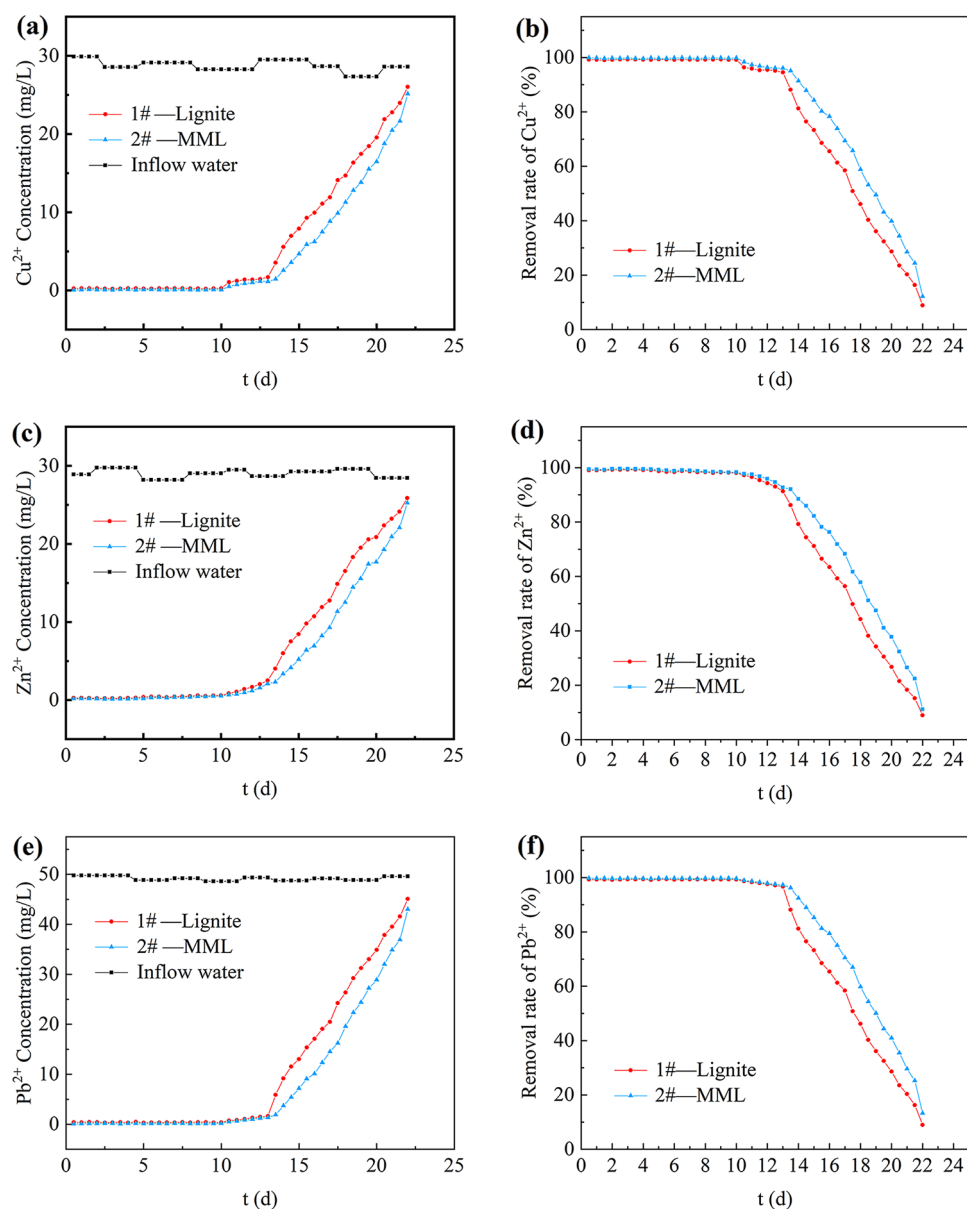


Figure 7. Removal effect of heavy metal ion. (a) Cu^{2+} concentration of effluent; (b) removal rate of Cu^{2+} ; (c) Zn^{2+} concentration of effluent; (d) removal rate of Zn^{2+} ; (e) Pb^{2+} concentration of effluent; (f) removal rate of Pb^{2+} .

solution is low, the precipitate of $\text{Zn}(\text{OH})_2$ adsorbed on the surface of MML is dissolved, and Zn^{2+} re-enter the solution.

Dynamic experimental analysis. The dynamic removal effects of lignite and MML on Cu^{2+} , Zn^{2+} and Pb^{2+} with time were shown in Fig. 7. The dynamic removal effects of both lignite and MML on Cu^{2+} , Zn^{2+} and Pb^{2+} shows a similar trend (Fig. 7). Heavy metal ions are removed rapidly in the first 13 days, with removal rates of Cu^{2+} , Zn^{2+} and Pb^{2+} exceeding 95, 92 and 97%, respectively. Then the removal rates gradually decreases from the 13th day to the 22nd day, and the removal rates is only about 10% at the 22nd day. This phenomenon is attributed to the fact that there are enough binding sites on the surfaces of adsorbent lignite and MML for metal ions to occupy at the initial stage, which make the adsorption process easier. However, the number of effective adsorption sites on the surfaces of lignite and MML gradually consumes with time, resulting in a decrease in the removal rates. During the whole dynamic removal cycle, the average removal rates of Cu^{2+} , Zn^{2+} and Pb^{2+} by lignite are 78.00, 76.97 and 78.65%, respectively, and the average removal rates of the studied heavy metal ions by MML are 82.83, 81.57 and 83.50%, respectively. Apparently, magnetic modification increases the adsorption capacity of heavy metal ions by the lignite. This may be because the surface of MML is loaded with Fe_3O_4 particles, which increases the specific surface area of lignite²³. In addition, the adsorption capacity of the three heavy

metal ions in AMD by lignite and MML is as follows: $Pb^{2+} > Cu^{2+} > Zn^{2+}$, which is the same as the result reported by Jellali et al.¹⁸.

Characterization analysis. *SEM analysis.* SEM detection results of lignite and MML before and after the dynamic test are shown in Fig. 8. From Fig. 8a,b, it appears that the raw lignite presents a smooth and porous surface with a larger pore size. However, MML presents a slightly rough surface, which is mainly because the successful loading of Fe_3O_4 on the lignite surface. A large number of Fe_3O_4 particles were scattered on the surface of lignite, which increased the specific surface area of the lignite and facilitated the removal of Cu^{2+} , Zn^{2+} and Pb^{2+} by MML. From Fig. 8c, d, surface voids of lignite after adsorption of Cu^{2+} , Zn^{2+} and Pb^{2+} are filled. Compared with lignite, the granular material on the surface of MML was significantly increased, indicating that more sediment was generated on the surface of MML.

XRD analysis. The XRD test results of lignite and MML before dynamic test are shown in Fig. 8e. The XRD patterns of lignite have relatively wide diffraction peaks (Fig. 8e). The diffraction peaks at $2\theta = 20.6^\circ$, 26.70° , 39.5° and $2\theta = 23.1^\circ$, 33.0° were caused by SiO_2 and S in lignite, respectively. Compared with lignite, the number of wide peaks in MML XRD pattern decreased, and the characteristic peaks of SiO_2 and S disappeared. New diffraction peaks appeared at $2\theta = 30.09^\circ$, 35.42° , 43.05° , 56.93° and 62.52° , showing the diffraction planes of (220), (311), (400), (511) and (440). These diffraction planes are consistent with the standard XRD data of cubic Fe_3O_4 , and it can be inferred that Fe_3O_4 is successfully deposited on the surface of lignite²⁴. The significant surface phase changes are consistent with SEM, further verifying that the surface of MML became rougher due to the presence of Fe_3O_4 . The rough surface of MML led to an increase in specific surface area, which is conducive to the adsorption of heavy metal ions.

The XRD test results of lignite and MML after dynamic test are shown in Fig. 8f. By comparing the XRD patterns of lignite and MML before and after the dynamic test, new diffraction peaks appeared at $2\theta = 11.3^\circ$, 11.8° , 19.5° and 22.5° after the dynamic test, corresponding to $C_4H_6O_4Zn$ diffraction. New diffraction peaks appeared at $2\theta = 31.4^\circ$ and 43.2° , corresponding to Pb and Cu elemental diffraction, respectively. $C_4H_6O_4Zn$ was a metal compound formed by electrostatic interaction and coordination between Zn^{2+} and functional groups in humic acid. Cu and Pb were generated by the reduction of Cu^{2+} and Pb^{2+} , which indicates that the adsorption of Cu^{2+} , Zn^{2+} and Pb^{2+} by lignite is chemisorption. Combined with the analysis results of adsorption kinetics, the adsorption process of heavy metal ions by lignite involves physisorption and chemisorption, but mainly physisorption. After the reaction, new diffraction peaks appeared at $2\theta = 30.1^\circ$, 35.5° , 43.1° , 57.0° and 62.6° , corresponding to the crystal plane diffraction of $CuFe_2O_4$, and new diffraction peaks appeared at $2\theta = 35.3^\circ$ and 62.3° , corresponding to the crystal plane diffraction of $ZnFe_2O_4$. It shows that Cu^{2+} and Zn^{2+} in AMD solution co-precipitated with Fe_3O_4 , and the resulting sediments were attached to the surface of MML in the form of $CuFe_2O_4$ and $ZnFe_2O_4$. New diffraction peaks appeared at $2\theta = 20.2^\circ$ and 37.7° , corresponding to the crystal surface diffraction of $Zn(OH)_2$. The occurrence of $Zn(OH)_2$ may be due to the increase of pH value caused by the consumption of H^+ in the reaction process. In addition, PbS diffraction peaks appeared at $2\theta = 30.1^\circ$ and 43.1° . This may be due to the fact that lignite contains a certain amount of S^{2-} , which is dissolved and released as the reaction progresses and reacted with the free Pb^{2+} in AMD. The results show that MML can remove Pb^{2+} and S^{2-} at the same time, and prevent the oxidation of S^{2-} in lignite to SO_4^{2-} , causing secondary pollution. The appearance of phases such as $CuFe_2O_4$, $ZnFe_2O_4$, $Zn(OH)_2$ and PbS confirms that the adsorption process of Cu^{2+} , Zn^{2+} and Pb^{2+} by MML is mainly chemisorption.

FTIR analysis. The lignite and MML before and after the dynamic test were taken for FTIR detection, and the results are shown in Fig. 8g,h. The peaks of lignite and MML at 3400 cm^{-1} was caused by O–H stretching vibrations of carboxylic acid groups, and the peak at 2920 cm^{-1} was attributed to the presence of $-CH_2$ in the stretching of aliphatic compounds, and the peak at 1600 cm^{-1} was related to the stretching vibrations of carboxylic acid functional groups⁴⁷ (Fig. 8f, h). Some peaks of lignite changed after magnetic modification, especially the generation of new peaks at 584 cm^{-1} , was attributed to Fe–O stretching vibrations of Fe_3O_4 particles⁴⁸. It shows that Fe_3O_4 was successfully loaded onto the lignite surface, which is consistent with the XRD results.

After the dynamic test, the peak position and intensity of some functional groups in lignite changed slightly. For instance, the peaks value at 3384 , 2921 and 1599 cm^{-1} moved to 3392 , 2923 and 1597 cm^{-1} , respectively. It shows that the adsorption of Cu^{2+} , Zn^{2+} and Pb^{2+} by lignite is due to physisorption under van der Waals forces²⁸. The peak value of MML at 586 cm^{-1} shifted to 575 cm^{-1} , indicating the possibility of Fe–O combining with Cu^{2+} and Zn^{2+} through Fe–O–Cu and Fe–O–Zn. In addition, the peak shape of the hydroxyl group corresponding to 1111 – 1270 cm^{-1} also changed, which may be due to the reaction of Zn^{2+} and OH^- to produce $Zn(OH)_2$ precipitation. These phenomena are consistent with XRD results. The stretching vibration of Zn^{2+} by hydroxyl group of carboxylic acid group in lignite generated metal compound $C_4H_6O_4Zn$, and the stretching vibration of Cu^{2+} and Zn^{2+} by Fe–O of Fe_3O_4 particles in MML generated $CuFe_2O_4$ and $ZnFe_2O_4$.

Compare the removal of Cu^{2+} , Zn^{2+} and Pb^{2+} by different adsorbents. Although the Langmuir model assumes that monolayer adsorption occurs on the uniform adsorbent surface and there is no interaction between adsorbates, many researchers have used Langmuir constant q_m to evaluate the adsorption capacity of adsorbents. To compare the maximum adsorption capacity of Cu^{2+} , Zn^{2+} and Pb^{2+} during the adsorption process, various adsorbents for Cu^{2+} , Zn^{2+} and Pb^{2+} removal were prepared, as shown in Table 4. It shows that lignite and MML have higher adsorption capacity in removing Cu^{2+} , Zn^{2+} and Pb^{2+} . The maximum monolayer adsorption capacity of lignite are 13.3618 , 14.7929 and 17.5274 mg/g , respectively, and the maximum monolayer adsorption capacities of MML for Cu^{2+} , Zn^{2+} and Pb^{2+} are 16.2127 , 15.8053 and 18.3870 mg/g , respectively. This

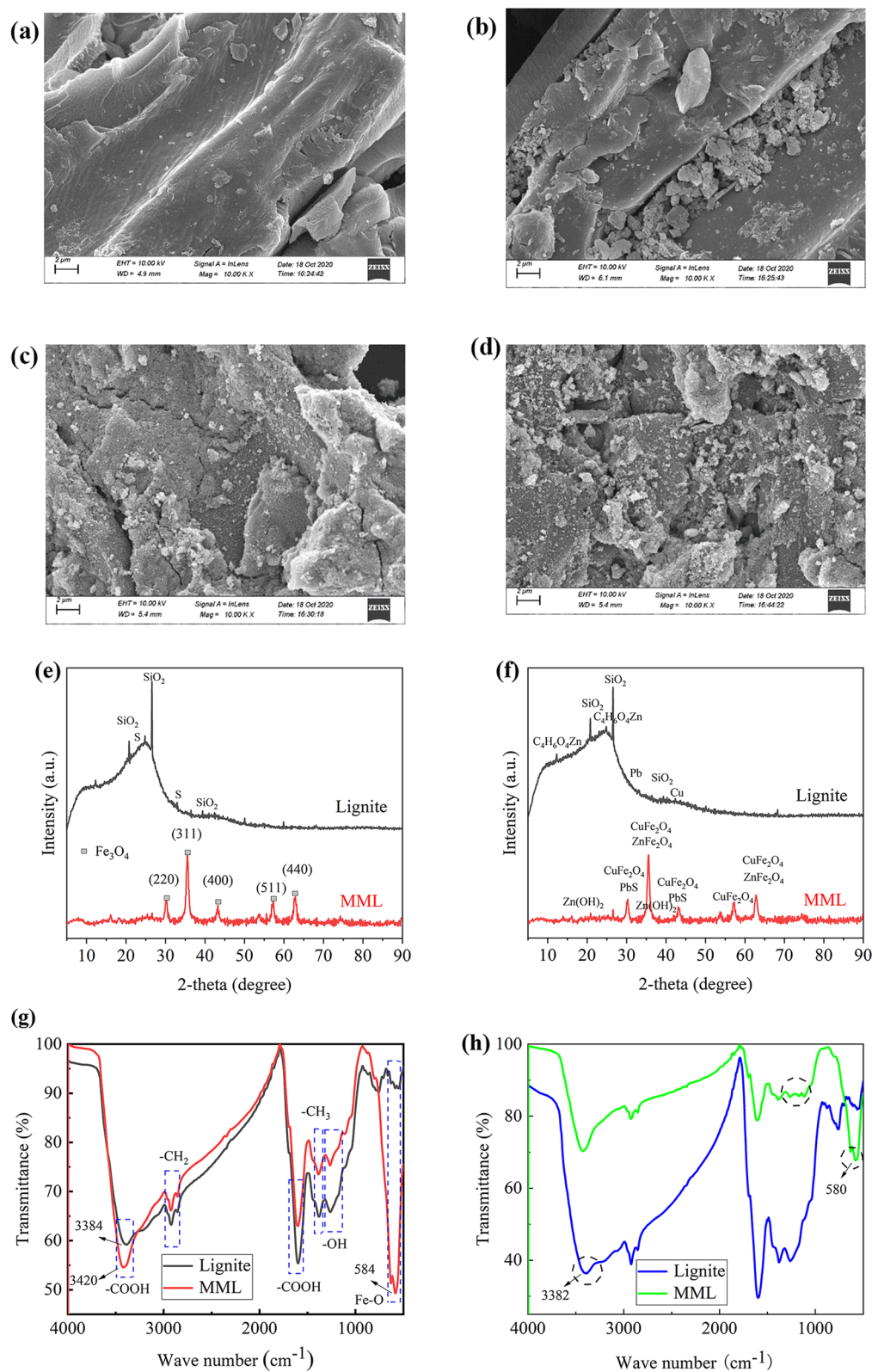


Figure 8. Characterization for adsorption of Cu^{2+} , Zn^{2+} and Pb^{2+} onto different samples: lignite; MML. SEM images for before adsorption: (a) lignite; (b) MML. SEM images for after adsorption: (c) lignite; (d) MML. XRD patterns of lignite and MML: (e) before adsorption; (f) after adsorption. FTIR spectra of lignite and MML: (g) before adsorption, (h) after adsorption.

Heavy metal	Adsorbent	Does (g/L)	Adsorption capacity (mg/g)	References
Cu ²⁺	Hydroxyapatite	10.00000	10.58000	49
	Attapulgit/(La + Fe)	8.00000	7.15610	50
	Sewage sludge activated carbon	4.00000	4.04000	51
	Lignite	4.00000	13.36180	This work
	MML		16.21270	
Zn ²⁺	Red earth	10.00000	8.74000	52
	Functionalized wool	5.00000	1.09000	53
	Sugarcane-bagasse ash	10.00000	3.34798	54
	Lignite	4.00000	14.79290	This work
	MML		15.80530	
Pb ²⁺	Carbonised sugarcane bagasse	10.00000	7.29930	55
	Attapulgit/(La + Fe)	8.00000	4.00270	50
	Mangrove bark (<i>Rhizopora mucronata</i>)	16.00000	18.28100	56
	Lignite	4.00000	17.52740	This work
	MML		18.38700	

Table 4. Comparison of the maximum monolayer adsorption capacities of Cu²⁺, Zn²⁺ and Pb²⁺ on various adsorbents.

indicates that MML is a potential adsorbent for Cu²⁺, Zn²⁺ and Pb²⁺ adsorption from AMD. On the other hand, the optimum amount (4 g/L) of MML is lower than that of other sorbents. It shows that MML can be used as a low-cost adsorbent to remove Cu²⁺, Zn²⁺ and Pb²⁺ from AMD (Table 4).

Conclusion

1. The best adsorption conditions for Cu²⁺, Zn²⁺ and Pb²⁺ by lignite and MML were pH = 4, adsorbent dosage 4 g/L and temperature 25°C. Under the same metal concentration conditions, the adsorption capacity and removal rates of Cu²⁺, Zn²⁺ and Pb²⁺ by MML were higher than that of lignite. When the concentration of heavy metal ions in AMD solution was higher, MML had greater adsorption potential than lignite.
2. The isothermal adsorption of Cu²⁺, Zn²⁺ and Pb²⁺ by lignite and MML was consistent with the Langmuir model, indicating that the adsorption was consistent with the monolayer layer adsorption process. The adsorption processes of Cu²⁺, Zn²⁺ and Pb²⁺ by lignite obeyed the Quasi first-order kinetic model, indicating that the adsorption process was dominated by physisorption, and the fitted equations were: $y = 9.2602 \cdot (1 - e^{-0.00607x})$, $y = 10.2839 \cdot (1 - e^{-0.00468x})$, and $y = 11.8456 \cdot (1 - e^{-0.01265x})$, respectively. The adsorption process of MML obeyed the Quasi second-order kinetic model, which indicates that the adsorption process was dominated by chemisorption and the adsorption rate was affected by the coordination between the surface active site of adsorbent and the heavy metal ions, and the fitted equations are: $y = 0.09599x + 8.81861$, $y = 0.09333x + 10.01582$, $y = 0.05103x + 5.02836$. The fitting results of Intra-particle diffusion model showed that the adsorption processes of lignite and MML was jointly controlled by multiple adsorption stages. The Elovich model and desorption experiments confirmed that the adsorption process of Cu²⁺, Zn²⁺ and Pb²⁺ by MML was mainly chemisorption. The adsorption thermodynamics showed that the adsorption of Cu²⁺ and Zn²⁺ by lignite and MML was spontaneous and endothermic, while the adsorption of Pb²⁺ was exothermic.
3. The dynamic experimental results showed that the removal effect of heavy metal ions by lignite was significantly better than that of lignite. The average removal rates of Cu²⁺, Zn²⁺ and Pb²⁺ by lignite were 78.00, 76.97 and 78.65%, respectively, and the average removal rates of the studied heavy metal ions by MML were 82.83, 81.57 and 83.50%, respectively. In addition, the adsorption capacity of the three heavy metal ions in AMD by lignite and MML is as follows: Pb²⁺ > Cu²⁺ > Zn²⁺.
4. From SEM, XRD and FTIR tests, it showed that Fe₃O₄ was successfully loaded onto the lignite surface during the magnetic modification process. SEM test showed that the surface morphology of lignite was rougher after magnetic modification, and more sediment was generated on MML surface after the reaction. XRD results showed that Lignite and MML removed Cu²⁺, Zn²⁺ and Pb²⁺ from AMD in different forms. FTIR results showed that the adsorption process of Cu²⁺, Zn²⁺ and Pb²⁺ by MML was related to the O–H stretching vibration of carboxylic acid ions and Fe–O stretching vibration of Fe₃O₄ particles.
5. The raw lignite has the characteristics of low cost and wide source. Using magnetic modification method to modify lignite can not only improve the adsorption capacity of the lignite, but also solve the problem that the lignite is difficult to separate from the solution. In this paper, a new modification method of lignite was proposed, which verified the feasibility of MML in the treatment of AMD, and provided a basis for the adsorption and use of MML.

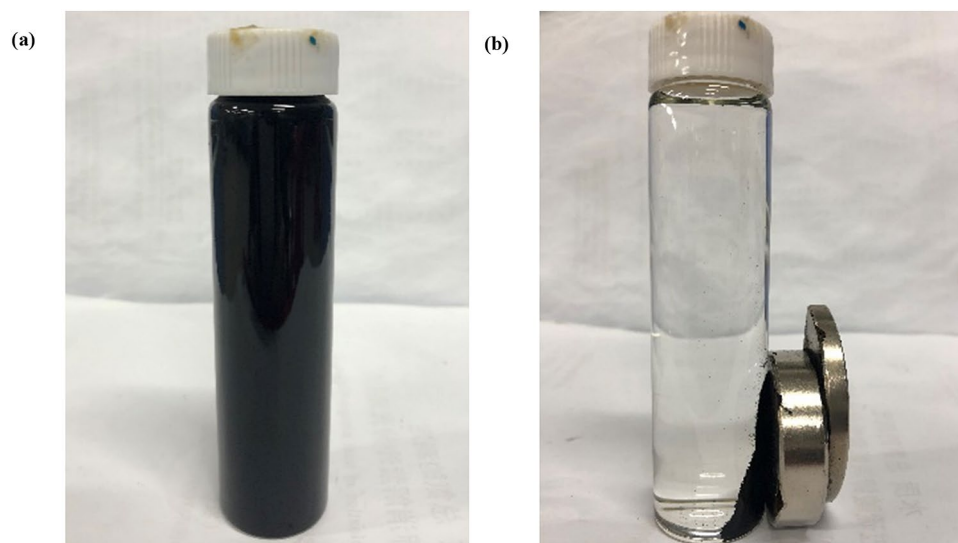


Figure 9. Comparison of solid–liquid separation effects between lignite and MML. (a) Lignite; (b) MML.

Materials and methods

Materials and chemicals. The lignite was purchased from Shanxi Fuhong Mineral Products Co., Ltd. $\text{FeSO}_4 \cdot 7\text{H}_2\text{O}$, HNO_3 , $\text{Fe}_2(\text{SO}_4)_3$, $\text{NH}_3 \cdot \text{H}_2\text{O}$, $\text{CuSO}_4 \cdot 5\text{H}_2\text{O}$, $\text{ZnSO}_4 \cdot 7\text{H}_2\text{O}$, $\text{Pb}(\text{NO}_3)_2$, Na_2SO_4 , H_2SO_4 were purchased from Liaoning Quanrui Reagent Co., LTD. Chemicals and reagents were analytical grade.

Adsorbent preparation. Lignite: Lignite was pulverized with a high-speed mill and screened out with a diameter of 250 mesh (58 μm). The lignite was immersed in deionized water for 2–3 times to remove impurities, and then dried at 60 $^\circ\text{C}$ for 24 h as the raw material.

MML: The chemical co-precipitation method is used to magnetically modify the lignite, that is, to load Fe_3O_4 magnetic particles on the surface of the lignite⁵⁷. The formation reaction formula of Fe_3O_4 is as follows.



The molar ratio of Fe^{3+} to Fe^{2+} substance was set to 2:1 (i.e. 1.31 g $\text{FeSO}_4 \cdot 7\text{H}_2\text{O}$ and 1.88 g $\text{Fe}_2(\text{SO}_4)_3$). 200 mL and 0.7 mol/L iron ion solution was prepared and placed in a thermostatic water bath at 60 $^\circ\text{C}$. Weigh 10 g lignite and add it to iron solution, stir it for 1 h under the action of an electric stirrer with speed regulation at 350 r/min, then add concentrated ammonia water with mass fraction of 25% drop by drop to pH value of 9, continue to stir for 1 h, and stand for 2 h for aging. The resulting precipitate was repeatedly cleaned with deionized water to make the supernatant neutral and then separated by magnets to obtain the magnetic material. The magnetic material was dried in a vacuum drying oven for 12 h to obtain MML. The comparison of solid–liquid separation between lignite and MML in Fig. 9.

Heavy metal ions solutions preparation and analysis. $\text{CuSO}_4 \cdot 5\text{H}_2\text{O}$, $\text{ZnSO}_4 \cdot 7\text{H}_2\text{O}$ and $\text{Pb}(\text{NO}_3)_2$ were used to prepare Cu^{2+} , Zn^{2+} and Pb^{2+} standard solutions, respectively. Metal concentrations were measured thorough an atomic absorption spectrometer (AAS) with an air-acetylene flame (Hitachi-Z2000, Japan). The wavelengths used for the analysis of the Cu^{2+} , Zn^{2+} , and Pb^{2+} were 324.8, 213.9, and 283.3 nm, respectively. The pH values of the solutions were adjusted by using 3% nitric acid or sodium hydroxide.

Experimental methods. *Adsorption condition optimization experiment.* Prepared a Cu^{2+} standard solution with a concentration of 30 mg/L. Added a certain amount of lignite and MML into 250 mL conical flasks containing 250 mL Cu^{2+} standard solution. Placed the conical flasks in a constant tremors shaking at 150 r/min, adsorb for 180 min, and then sample with a pipette gun. The samples were filtered through a 0.45 μm microporous membrane before analysis with AAS. Calculated the removal rates and adsorption amounts of heavy metal ions by Eqs. (12) and (13)⁵⁸. All the experiments were repeated three times, and the average values were taken as the final measured values. The research was carried out by changing the pH value of the solution (2–4), adsorbent dose (2–6 g/L) and temperature (298.15, 308.15 and 318.15 K). The test conditions and process of the Zn^{2+} standard solution with a concentration of 30 mg/L and the Pb^{2+} standard solution with a concentration of 50 mg/L were exactly the same as the Cu^{2+} adsorption test.

$$E = \frac{C_0 - C_t}{C_0} \times 100\% \quad (12)$$

$$q_e = \frac{(C_0 - C_e)V}{M} \quad (13)$$

where E is the removal rate (%), C_0 is the initial mass concentration (mg/L), C_t is the mass concentration of the remaining metal ions in the solution at time t (mg/L), q_e is the adsorption amount at equilibrium (mg/g), C_e is the mass concentration of the remaining metal ions in the solution at equilibrium (mg/L), V is the volume of the solution (L), and M is the mass of the adsorbent material (g).

Adsorption isotherm experiment. Prepared Cu^{2+} , Zn^{2+} and Pb^{2+} solutions with initial concentrations of 10, 30, 50, 70 and 90 mg/L, respectively, and adjusted the pH values of each solution to 4. Taken 250 mL of Cu^{2+} , Zn^{2+} and Pb^{2+} solutions with different concentrations in a 250 mL conical flask, and added 1 g lignite or MML into the solutions. Placed the conical flasks in a constant tremors shaking at 25 °C, 150 r/min, adsorbed for 180 min, and then sampled with a pipette gun. The samples were filtered through a 0.45 μm microporous membrane before analysis with AAS. Calculated the removal rates and adsorption amounts of heavy metal ions by Eqs. (12) and (13). All the experiments were repeated three times, and the average values were taken as the final measured values.

Adsorption kinetics experiment. Prepared a Cu^{2+} standard solution with a concentration of 30 mg/L and adjust the pH value to 4. Weighed 1 g each of lignite and MML, and added them to two 250 mL conical flasks containing 250 mL of 30 mg/L Cu^{2+} standard solution. Placed the conical flasks in a constant tremors shaking at 25 °C and 150 r/min to desorb. At intervals (5, 10, 15, 30, 60, 90, 120 and 180 min), measured the Cu^{2+} concentrations thorough AAS. Calculated the removal rates and adsorption amounts. The test conditions and process of the Zn^{2+} standard solution with a concentration of 30 mg/L and the Pb^{2+} standard solution with a concentration of 50 mg/L were exactly the same as the Cu^{2+} adsorption test. All the experiments were repeated three times and the average values were taken as the final measured values.

Adsorption thermodynamics experiment. Prepared a Cu^{2+} standard solution with a concentration of 30 mg/L and adjust the pH value to 4. Weighed 1 g of lignite or MML and added it to a 250 mL conical flask containing 250 mL of 30 mg/L Cu^{2+} standard solution. Placed the conical flasks in constant tremors shaking at 150 r/min for 180 min in different temperature (298.15, 308.15 and 318.15 K), and then sample with a pipette gun. The samples were filtered through a 0.45 μm microporous membrane before analysis with AAS. Calculated the removal rates and adsorption amounts of heavy metal ions by Eqs. (12) and (13). The test conditions and process of the Zn^{2+} standard solution with a concentration of 30 mg/L and the Pb^{2+} standard solution with a concentration of 50 mg/L were exactly the same as the Cu^{2+} adsorption test. All the experiments were repeated three times, and the average values were taken as the final measured values.

Desorption experiment. Prepared a Cu^{2+} standard solution with a concentration of 30 mg/L and adjust the pH value to 4. Weighed 1 g of MML and added it to a 250 mL conical flask containing 250 mL of 30 mg/L Cu^{2+} standard solution. Placed the conical flasks in a constant tremors shaking at 25 °C and 150 r/min to oscillate and react for 180 min before analysis with AAS. Used a magnet to take out the reacted MML. The collected MML was washed several times with deionized water and then added to a 250 mL conical flask containing 250 mL of 0.1 mol/L H_2SO_4 solution. Placed the conical flasks in a constant tremors shaking at 25 °C and 150 r/min to desorb for 180 min before analysis with AAS. Calculated the desorption amounts and desorption rates by Eqs. (14) and (15)⁵⁹. The test conditions and process of the Zn^{2+} standard solution with a concentration of 30 mg/L and the Pb^{2+} standard solution with a concentration of 50 mg/L were exactly the same as the Cu^{2+} adsorption test. All the experiments were repeated three times and the average values were taken as the final measured values.

$$q_d = \frac{CV}{M} \times 100\% \quad (14)$$

$$TD = \frac{q_d}{q_e} \times 100\% \quad (15)$$

where q_e is the adsorption capacity at equilibrium (mg/g), Q_d is desorption amount (mg/g), C is the concentration of heavy metal ions in ethanol solution at 180 min (mg/L), V is the volume of solution (L), M is the mass of adsorption material (g), and TD is desorption rate (%). If $TD > 50\%$, the adsorption is physical adsorption. If $TD < 50\%$, chemisorption.

Dynamic experiment. Two Plexiglas's tubes with an inner diameter of 40 mm and a height of 250 mm were filled with lignite and MML respectively. Glass beads with a height of 25 mm and a diameter of 3–5 mm were arranged at the top and bottom of the dynamic column, and 100 mm high lignite was filled in the middle of #1 Plexiglas tube, and 100 mm high MML was filled in the middle of #2 Plexiglas tube. According to the results of the static beaker experiments, prepared the AMD with Cu^{2+} and Zn^{2+} concentration of 30 mg/L and Pb^{2+} concentration of 50 mg/L, and adjusted the pH value to 4. The overall operation mode adopted "bottom in and top out" continuous operation, and the inlet water flow rate was adjusted to 0.556 mL/min by peristaltic pump and flowmeter. The experimental device was shown in Fig. 10. The two groups of dynamic columns were operated at room temperature for 22 days, and samples were taken every 12 h. After the samples were filtered by 0.45 μm

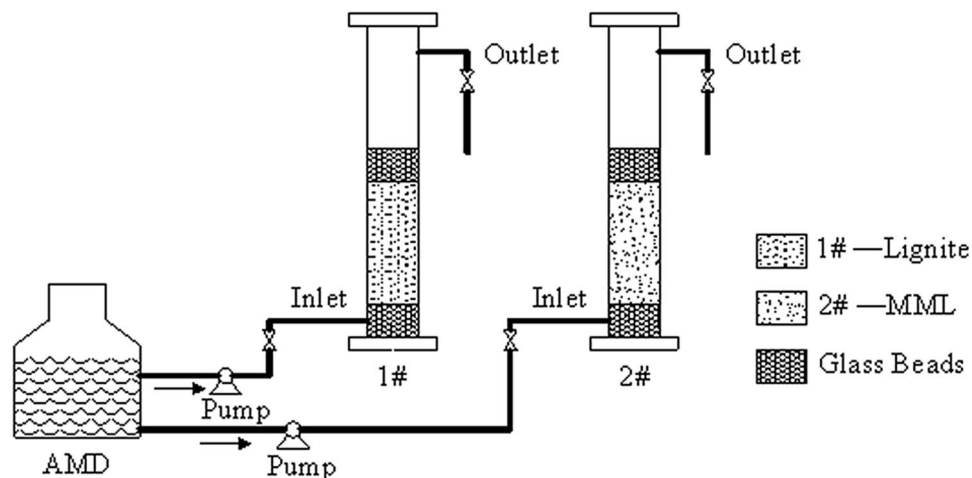


Figure 10. Dynamic test running device diagram.

microporous membrane, the concentrations of Cu^{2+} , Zn^{2+} and Pb^{2+} in the solution were determined through AAS.

Adsorbent characterization. Lignite and MML before and after dynamic test were characterized by various techniques. SEM (Zeiss-Sigma 500, GER) was used to analyze the morphology and surface morphology of the adsorbent before and after adsorption. The phase and structure of the adsorbent were determined by XRD (Rigaku-Smartlab9, Japan). FTIR (Thermo Fisher-Nicolet iS5, USA) was recorded in the $500\text{--}4000\text{ cm}^{-1}$ range to study the surface functional groups before and after adsorption.

Data availability

All data generated or analyzed during this study are included in this published article.

Received: 25 September 2021; Accepted: 7 January 2022

Published online: 26 January 2022

References

- Dong, Y. R. *et al.* Dynamic experimental study on treatment of acid mine drainage by bacteria supported in natural minerals. *Energies* **13**(2), 439. <https://doi.org/10.3390/en13020439> (2020).
- Akinpelu, E. A., Ntwampe, S. K.O., Fosso-Kankeu, E., Nchu, F. & Angadam, J. O. Performance of microbial community dominated by *Bacillus* spp. in acid mine drainage remediation systems: A focus on the high removal efficiency of SO_4^{2-} , Al^{3+} , Cd^{2+} , Cu^{2+} , Mn^{2+} , Pb^{2+} , and Sr^{2+} . *Heliyon*. **7**(6), e07241. <https://doi.org/10.1016/j.heliyon.2021.e07241> (2021).
- Ge, F., Li, M. M., Ye, H. & Zhao, B. X. Effective removal of heavy metal ions Cd^{2+} , Zn^{2+} , Pb^{2+} , Cu^{2+} from aqueous solution by polymer-modified magnetic nanoparticles. *J. Hazard. Mater.* **211–212**, 366–372. <https://doi.org/10.1016/j.jhazmat.2011.12.013> (2012).
- Magagane, N., Masindi, V., Ramakokovhu, M. M., Brendon, S. M. & Lilith, M. K. Facile thermal activation of non-reactive cryptocrystalline magnesite and its application on the treatment of acid mine drainage. *J. Environ. Manage.* **236**, 499–509. <https://doi.org/10.1016/j.jenvman.2019.02.030> (2019).
- Matlock, M. M., Howerton, B. S. & Atwood, D. A. Chemical precipitation of heavy metals from acid mine drainage. *Water Res.* **36**, 4757–4764. [https://doi.org/10.1016/S0043-1354\(02\)00149-5](https://doi.org/10.1016/S0043-1354(02)00149-5) (2002).
- Nogueira, E. W., Godoi, L., Yabuki, L., Brucha, G. & Damianovic, M. Sulfate and metal removal from acid mine drainage using sugarcane vinasse as electron donor: Performance and microbial community of the down-flow structured-bed bioreactor. *Biores. Technol.* **330**, 124968. <https://doi.org/10.1016/j.biortech.2021.124968> (2021).
- Yan, X. X. *et al.* Heavy metals uptake and translocation of typical wetland plants and their ecological effects on the coastal soil of a contaminated bay in Northeast China. *Sci. Total Environ.* **803**, 149871. <https://doi.org/10.1016/j.scitotenv.2021.149871> (2021).
- Sheoran, A. S. & Sheoran, V. Heavy metal removal mechanism of acid mine drainage in wetlands: A critical review. *Miner. Eng.* **19**, 105–116. <https://doi.org/10.1016/j.mineng.2005.08.006> (2006).
- Zhou, G. Y., Luo, J. M., Liu, C. B., Chu, L. & Crittenden, J. Efficient heavy metal removal from industrial melting effluent using fixed-bed process based on porous hydrogel adsorbents. *Water Res.* **131**, 246–254. <https://doi.org/10.1016/j.watres.2017.12.067> (2018).
- Zhao, T. T. *et al.* Mechanism study of Cr(III) immobilization in the process of Cr(VI) removal by Huolinhe lignite. *Fuel Process. Technol.* **152**, 375–380. <https://doi.org/10.1016/j.fuproc.2016.06.037> (2016).
- Zendelska, A., Golomeova, M., Golomeov, B. & Krstev, B. Removal of zinc ions from acid aqueous solutions and acid mine drainage using zeolite-bearing tuff. *Mine Water Environ.* **38**(1), 187–196. <https://doi.org/10.1007/s10230-018-0560-y> (2018).
- Lin, H. *et al.* Adsorption of copper ions from acid mine drainage using spent shiitake substrate. *Chin. J. Eng.* **35**(9), 1119–1125. <https://doi.org/10.13374/j.issn1001-053x.2013.09.015> (2013).
- Yang, Y., Chen, T. H., Li, P., Xie, Q. Q. & Zhan, X. M. Cu removal from acid mine drainage by modified pyrite: Batch and column experiments. *Mine Water Environ.* **36**(3), 371–378. <https://doi.org/10.1007/s10230-016-0421-5> (2017).
- Lin, H., Zhang, X. P., Dong, Y. B. & Zheng, Q. Q. Adsorbing Pb^{2+} and Zn^{2+} from Acidmine Drainage by Coffee Grounds. *J. Tongji Univ. (Nat. Sci.)*. **42**(9), 1365–1371. <https://doi.org/10.3969/j.issn.0253-374x.2014.09.010> (2014).
- Mohan, D. & Chander, S. Removal and recovery of metal ions from acid mine drainage using lignite—A low cost sorbent. *J. Hazard. Mater.* **137**(3), 1545–1553. <https://doi.org/10.1016/j.jhazmat.2006.04.053> (2006).

16. Smilek, J., Sedláček, P., Kalina, M. & Klučáková, M. On the role of humic acids' carboxyl groups in the binding of charged organic compounds. *Chemosphere* **138**, 503–510. <https://doi.org/10.1016/j.chemosphere.2015.06.093> (2015).
17. Murata, S., Hosokawa, M., Kidena, K. & Nomura, M. Analysis of oxygen-functional groups in brown coals. *Fuel Process. Technol.* **67**(3), 231–243. [https://doi.org/10.1016/S0378-3820\(00\)00102-8](https://doi.org/10.1016/S0378-3820(00)00102-8) (2000).
18. Jellali, S., Azzaz, A. A., Jeguirim, M., Hamdi, H. & Mlayah, A. Use of lignite as a low-cost material for cadmium and copper removal from aqueous solutions: Assessment of adsorption characteristics and exploration of involved mechanisms. *Water* **13**, 164. <https://doi.org/10.3390/w13020164> (2021).
19. Munir, M. A. M. *et al.* Interactive assessment of lignite and bamboo-biochar for geochemical speciation, modulation and uptake of Cu and other heavy metals in the copper mine tailing. *Sci. Total Environ.* **779**, 146536. <https://doi.org/10.1016/j.scitotenv.2021.146536> (2021).
20. Sakthivel. *et al.* Switching the hydrophobic Neyveli lignite into hydrophilic type by surface modification and its subsequent use for removing Cr(VI)/F—from artificial pollutant. *Fuel*. **298**, 120787. <https://doi.org/10.1016/j.fuel.2021.120787> (2021).
21. Regassa, B., Beteley, T., Tariku, A. & Bayisa, D. Investigation of the adsorption performance of acid treated lignite coal for Cr(VI) removal from aqueous solution. *Environ. Challenges*. **4**, 100091. <https://doi.org/10.1016/j.envc.2021.100091> (2021, prepublsh).
22. He, Q. Q. *et al.* Adsorption of direct yellow brown D3G from aqueous solution using loaded modified low-cost lignite: Performance and mechanism. *Environ. Technol.* **42**(11), 1642–1651. <https://doi.org/10.1080/09593330.2019.1675774> (2021).
23. Cheng, Z. H. *et al.* Preparation of magnetic Fe₃O₄ particles modified sawdust as the adsorbent to remove strontium ions. *Chem. Eng. J.* **209**, 451–457. <https://doi.org/10.1016/j.cej.2012.07.078> (2012).
24. Feng, G. R. *et al.* Magnetic natural composite Fe₃O₄-chitosan@bentonite for removal of heavy metals from acid mine drainage. *J. Colloid Interface Sci.* <https://doi.org/10.1016/j.jcis.2018.11.087> (2018).
25. Chen, L. F., Wu, X. R., Liu, C., Zhao, Y. M. & Huang, Q. Study on removal of Microcystis aeruginosa and Cr(VI) using attapulgite-Fe₃O₄ magnetic composite material (MCM). *Algal Res.* **60**, 102501. <https://doi.org/10.1016/j.algal.2021.102501> (2021).
26. Albadarin, A. B. *et al.* Kinetic and thermodynamics of chromium ions adsorption onto low-cost dolomite adsorbent. *Chem. Eng. J.* **179**, 193–202. <https://doi.org/10.1016/j.cej.2011.10.080> (2012).
27. Dehghani, M. H. *et al.* Process optimization and enhancement of pesticide adsorption by porous adsorbents by regression analysis and parametric modelling. *Sci. Rep.* **11**(1), 11719. <https://doi.org/10.1038/s41598-021-91178-3> (2021).
28. Yao, L., Esmaeili, H., Haghani, M. & Roco-Videla, A. Activated carbon/bentonite/Fe₃O₄ as novel nanobiocomposite for high removal of Cr(VI) ions. *Chem. Eng. Technol.* **44**(10), 1908–1918. <https://doi.org/10.1002/ceat.202100179> (2021).
29. Dehghani, M. H. *et al.* Process modeling of municipal solid waste compost ash for reactive red 198 dye adsorption from wastewater using data driven approaches. *Sci. Rep.* **11**(1), 11613. <https://doi.org/10.1038/s41598-021-90914-z> (2021).
30. Venkateswarlu, S., Yoon, M. & Kim, M. J. An environmentally benign synthesis of Fe₃O₄ nanoparticles to Fe₃O₄ nanoclusters: rapid separation and removal of Hg(II) from an aqueous medium. *Chemosphere*. **286**(P2), 131673. <https://doi.org/10.1016/j.chemosphere.2021.131673> (2022).
31. Chethan, P. D. & Vishalakshi, B. Adsorption efficiency of Cr (VI) by ethylene-1, 2-diamine-6-deoxychitosan. *Sep. Sci. Technol.* **50**(8), 1158–1165. <https://doi.org/10.1080/01496395.2014.967405> (2015).
32. Dehghani, M. H. *et al.* Statistical modelling of endocrine disrupting compounds adsorption onto activated carbon prepared from wood using CCD-RSM and DE hybrid evolutionary optimization framework: Comparison of linear vs non-linear isotherm and kinetic parameters. *J. Mol. Liq.* **302**, 112526. <https://doi.org/10.1016/j.molliq.2020.112526> (2020).
33. Azari, A., Yeganeh, M., Gholami, M. & Salari, M. The superior adsorption capacity of 2,4-Dinitrophenol under ultrasound-assisted magnetic adsorption system: Modeling and process optimization by central composite design. *J. Hazard. Mater.* **418**, 126348. <https://doi.org/10.1016/j.jhazmat.2021.126348> (2021).
34. Dehghani, M. H. *et al.* Adsorptive removal of cobalt(II) from aqueous solutions using multi-walled carbon nanotubes and γ-alumina as novel adsorbents: Modelling and optimization based on response surface methodology and artificial neural network. *J. Mol. Liquids*. **299**(C), 112154. <https://doi.org/10.1016/j.molliq.2019.112154> (2019).
35. Zhao, H. X. & Lang, Y. H. Adsorption behaviors and mechanisms of florfenicol by magnetic functionalized biochar and reed biochar. *J. Taiwan Inst. Chem. Eng.* **88**, 152–160. <https://doi.org/10.1016/j.jtice.2018.03.049> (2018).
36. Darvishmotevalli, M. *et al.* Evaluation of magnetic ZSM-5 composite performance in 2, 4 dichlorophenol removal from synthetic solutions: response surface method (RSM) modeling and isotherm, kinetic and thermodynamic studies. *Desalin. Water Treat.* **164**, 249–262. <https://doi.org/10.5004/dwt.2019.24451> (2019).
37. Kavitha, D. & Namasivayam, C. Experimental and kinetic studies on methylene blue adsorption by coir pith carbon. *Bioresour. Technol.* **98**(1), 14–21. <https://doi.org/10.1016/j.biortech.2005.12.008> (2007).
38. Hameed, B. H., Salman, J. M. & Ahmad, A. L. Adsorption isotherm and kinetic modeling of 2,4-D pesticide on activated carbon derived from date stones. *J. Hazard. Mater.* **163**(1), 121–162. <https://doi.org/10.1016/j.jhazmat.2008.06.069> (2009).
39. Ugwu, E.I., Othmani, A. & Nnaji, C.C. A review on zeolites as cost-effective adsorbents for removal of heavy metals from aqueous environment. *Int. J. Environ. Sci. Technol.* <https://doi.org/10.1007/s13762-021-03560-3> (2021).
40. Karabulut, S., Karabakan, A., Denizli, A. & Yurum, Y. Batch removal of copper(II) and zinc(II) from aqueous solutions with low-rank Turkish coals. *Sep. Purif. Technol.* **18**, 177–184. [https://doi.org/10.1016/S1383-5866\(99\)00067-2](https://doi.org/10.1016/S1383-5866(99)00067-2) (2000).
41. Shokoohi, R. *et al.* The sorption of cationic and anionic heavy metal species on the biosorbent of *Aspergillus terreus*: Isotherm, kinetics studies. *Environ. Prog. Sustain. Energy*. **39**(2), 1. <https://doi.org/10.1002/ep.13309> (2020).
42. Hong, Y. K. *et al.* Bottom ash modification via sintering process for its use as a potential heavy metal adsorbent: Sorption kinetics and mechanism. *Materials*. **14**(11), 3060. <https://doi.org/10.3390/ma14113060> (2021).
43. Dinh, H. T., Tran, N. T. & Trinh, D. X. Investigation into the adsorption of methylene blue and methyl orange by UiO-66-NO₂ nanoparticles. *J. Anal. Methods Chem.* **2021**, 5512174. <https://doi.org/10.1155/2021/5512174> (2021).
44. Sabzi, M., Ghafelebashi, A., Miri, M. & Mahdavinia, G. R. Preparation of Fe₃O₄ attached sepiolite/poly (vinyl alcohol) nanocomposite as a magnetically separable dye adsorbent. *J. Polym. Environ.* **28**, 211–219. <https://doi.org/10.1007/s10924-019-01600-1> (2020).
45. Mahmoudi, M. M. *et al.* Fluoride removal from aqueous solution by acid-treated clinoptilolite: isotherm and kinetic study. *Desalin. Water Treat.* **146**, 333–340. <https://doi.org/10.5004/dwt.2019.23625> (2019).
46. Zulfikar, M. A., Novita, E., Hertadi, R. & Djajanti, S. D. Removal of humic acid from peat water using untreated powdered eggshell as a low cost adsorbent. *Int. J. Environ. Sci. Technol.* **10**(6), 1357–1366. <https://doi.org/10.1007/s13762-013-0204-5> (2013).
47. Kong, Q. P., Wei, J. Y. & Wei, C. H. Fabrication of terminal amino hyperbranched polymer modified graphene oxide and its prominent adsorption performance towards Cr(VI). *J. Hazard. Mater.* **363**, 161–169. <https://doi.org/10.1016/j.jhazmat.2018.09.084> (2018).
48. Deng, S. B., Liu, H., Zhou, W., Huang, J. & Yu, G. Mn-Ce oxide as a high-capacity adsorbent for fluoride removal from water. *J. Hazard. Mater.* **186**(2–3), 1360–1366. <https://doi.org/10.1016/j.jhazmat.2010.12.024> (2011).
49. Ayodele, O. *et al.* Experimental and theoretical studies of the adsorption of Cu and Ni ions from wastewater by hydroxyapatite derived from eggshells. *Environ. Nanotechnol. Monit. Manag.* **15**, 439. <https://doi.org/10.1016/J.ENMM.2021.100439> (2021).
50. Shang, J. Q. *et al.* Adsorption of Pb(II) and Cu(II) by Attapulgite/(La+Fe). *In. J. Front. Eng. Technol.* **3**(2), 35–48. <https://doi.org/10.25236/IJFET.2021.030207> (2021).

51. Omar, K., Abed, M. A., Mouna, N., Mohamed, L. C. & Hamza, L. Response surface modeling and optimization of Ni(II) and Cu(II) ions competitive adsorption capacity by sewage sludge activated carbon. *Arab. J. Sci. Eng.* <https://doi.org/10.1007/S13369-021-05534-6> (2021).
52. Esmaeili, A. & Eslami, H. Adsorption of Pb(II) and Zn(II) ions from aqueous solutions by Red Earth. *MethodsX*. **7**, 100804. <https://doi.org/10.1016/j.mex.2020.100804> (2020).
53. Marjana, S. & Lidija, F. Z. Functionalized wool as an efficient and sustainable adsorbent for removal of Zn(II) from an aqueous solution. *Materials*. **13**(14), 3208. <https://doi.org/10.3390/ma13143208> (2020).
54. Rodríguez, D. J. M. *et al.* Laboratory adsorption studies on Ni(II) and Zn(II) solutions by sugarcane-bagasse ash. *Water Air Soil Pollut.* **232**(3), 1. <https://doi.org/10.1007/s11270-021-05046-x> (2021).
55. Oklo, A. D. *et al.* Adsorption isotherms and kinetics of Pb(II) and Cd(II) ions onto carbonised sugarcane bagasse. *Adv. Biochem.* **9**(3), 44–49 (2021).
56. Sudaryanto, Y., Anggorowati, A. A. & Sianto, M. E. Study of Pb(II) adsorption by Tannin based adsorbent from mangrove bark (*Rhizophora mucronata*). *J. Phys: Conf. Ser.* **1858**(1), 012086. <https://doi.org/10.1088/1742-6596/1858/1/012086> (2021).
57. Mohammad, S., Amirhossein, G., Mohammadjavad, M. & Gholam, R. M. Preparation of Fe₃O₄ ATTACHED sepiolite/poly(vinyl alcohol) nanocomposite as a magnetically separable dye adsorbent. *J. Polym. Environ.* **28**(1), 211–219. <https://doi.org/10.1007/s10924-019-01600-1> (2020).
58. Donatus, R. Adsorption of methylene blue dye using Fe₃O₄ magnetized natural zeolite adsorbent. *Jurnal Kimia Sains dan Aplikasi.* **24**(2), 51–57. <https://doi.org/10.14710/jksa.24.2.51-57> (2021).
59. Othmani, A., Kesraoui, A. & Seffen, M. Removal of phenol from aqueous solution by coupling alternating current with biosorption. *Environ. Sci. Pollut. Res. Int.* **28**(34), 46488–46503. <https://doi.org/10.1007/s11356-020-09976-7> (2021).

Author contributions

J.D., and Z.R. wrote this paper. J.D., Z.R., S.Z., Y.D., and S.F. finished the water quality analysis. J.D., Z.R., and S.Z. performed the long-term experiment. J.D., Z.R., Y.D., S.F., and H.L. performed the supplementary experiment. J.D., Z.R., H.L., and G.J. examined the grammar of the paper. All authors reviewed the manuscript.

Funding

This article was funded by National Natural Science Foundation of China (Grant no. 41672247), "Rejuvenating Liaoning Talents" youth top talent program of Liaoning Province (Grant no. XLYC1807159), discipline innovation team of Liaoning University of engineering and Technology (Grant no. LNTU20TD-21) and Liaoning Provincial Department of Education Project (Grant no. LJKZ0324).

Competing interests

The authors declare no competing interests.

Additional information

Correspondence and requests for materials should be addressed to Z.R.

Reprints and permissions information is available at www.nature.com/reprints.

Publisher's note Springer Nature remains neutral with regard to jurisdictional claims in published maps and institutional affiliations.



Open Access This article is licensed under a Creative Commons Attribution 4.0 International License, which permits use, sharing, adaptation, distribution and reproduction in any medium or format, as long as you give appropriate credit to the original author(s) and the source, provide a link to the Creative Commons licence, and indicate if changes were made. The images or other third party material in this article are included in the article's Creative Commons licence, unless indicated otherwise in a credit line to the material. If material is not included in the article's Creative Commons licence and your intended use is not permitted by statutory regulation or exceeds the permitted use, you will need to obtain permission directly from the copyright holder. To view a copy of this licence, visit <http://creativecommons.org/licenses/by/4.0/>.

© The Author(s) 2022